PROTEINS: Structure, Function, and Genetics 37:441–453 (1999)

The Crystal Structure of Triosephosphate Isomerase (TIM) From *Thermotoga maritima*: A Comparative Thermostability Structural Analysis of Ten Different TIM Structures

Dominique Maes,[1]* Johan P. Zeelen,[2] Narmada Thanki,[2] Nicola Beaucamp,[3] Marco Alvarez,[4] Minh Hoa Dao Thi,[1] Jan Backmann,[1] Joseph A. Martial,[4] Lode Wyns,[1] Rainer Jaenicke,[3] and Rik K. Wierenga[2,5]

[1]*Ultrastructure Unit, Vlaams Interuniversitair Instituut voor Biotechnologie, Vrije Universiteit Brussel, Sint-Genesiu-Rode, Belgium*

[2]*European Molecular Biology Laboratory, Heidelberg, Germany*

[3]*Institut für Biophysik und physikalische Biochemie, Universität Regensburg, Regensburg, Germany*

[4]*Laboratoire de Biologie Moléculaire et de Génie Génétique, Université de Liège, Liège, Belgium*

[5]*Department of Biochemistry, University of Oulu, Oulu, Finland*

ABSTRACT **The molecular mechanisms that evolution has been employing to adapt to environmental temperatures are poorly understood. To gain some further insight into this subject we solved the crystal structure of triosephosphate isomerase (TIM) from the hyperthermophilic bacterium *Thermotoga maritima* (TmTIM). The enzyme is a tetramer, assembled as a dimer of dimers, suggesting that the tetrameric wild-type phosphoglycerate kinase PGK-TIM fusion protein consists of a core of two TIM dimers covalently linked to 4 PGK units. The crystal structure of TmTIM represents the most thermostable TIM presently known in its 3D-structure. It adds to a series of nine known TIM structures from a wide variety of organisms, spanning the range from psychrophiles to hyperthermophiles. Several properties believed to be involved in the adaptation to different temperatures were calculated and compared for all ten structures. No sequence preferences, correlated with thermal stability, were apparent from the amino acid composition or from the analysis of the loops and secondary structure elements of the ten TIMs. A common feature for both psychrophilic and *T. maritima* TIM is the large number of salt bridges compared with the number found in mesophilic TIMs. In the two thermophilic TIMs, the highest amount of accessible hydrophobic surface is buried during the folding and assembly process. Proteins 1999;37:441–453.**

Key words: hydrophobicity; hyperthermophile; psychrophile; salt bridges; thermophile

INTRODUCTION

The thermal stability of proteins is the result of evolutionary pressure, depending on specific conditions of the environment. Consequently, large variations are observed if one compares proteins from psychrophilic organisms with ultrastable proteins from hyperthermophiles.[1] The strategies of thermal adaptation of proteins are still poorly understood. The study of protein thermal stability is important not only theoretically but also because of its potential biotechnological applications. For this purpose it is essential to obtain full understanding of the factors that influence stability and catalytic activity at low and high temperatures. Detailed structural information from proteins of protein families with representatives in psychrophilic and thermophilic organisms is essential. Only three structures of psychrophilic organisms have been reported so far.[2–4] In contrast, numerous examples of homologous enzymes from mesophiles, thermophiles, and hyperthermophiles have been documented.

Analysis of high resolution X-ray structures of proteins from a variety of thermophiles and hyperthermophiles has suggested that the adaptation to ambient temperatures, rather than being the consequence of one dominant type of interaction, arises from the addition of increments contributed by, e.g., salt bridges, decrease in accessible hydrophobic surface area, improved packing, helix stabilization, and higher states of subunit assembly.[1,5–7]

To gain further insight into the molecular mechanisms that nature uses to adapt to environmental temperatures, we have carried out a comparative structural analysis on triosephosphate isomerase (TIM; EC 5.3.1.1), a dimeric glycolytic enzyme consisting of two identical subunits, each about 250 residues long. It catalyzes the interconversion of dihydroxyacetone phosphate and D-glyceraldehyde-

Abbreviations: ASA, accessible surface area; AUC, analytical ultracentrifugation; BsTIM, *Bacillus stearothermophilus* TIM; ChTIM, chicken TIM; EcTIM, *Escherichia coli* TIM; HuTIM, human TIM; LeTIM, *Leishmania mexicana* TIM; PfTIM, *Plasmodium falciparum* TIM; PGK, phosphoglycerate kinase; TbTIM, *Trypanosoma brucei* TIM; TIM, triosephosphate isomerase; TmTIM, *Thermotoga maritima* TIM; VmTIM, *Vibrio marinus* TIM; YeTIM, yeast TIM.

Grant sponsor: European Union; Grant number: BIO4-CT96–0670; Grant sponsor: PRODEX ESA; Grant number: 1298/98/NL/VJ (IC); Grant sponsor: Actions de Recherche Concertées; Grant number: 95/00–193; Grant sponsor: Services Fédéreaux des Affaires Scientifiques Techniques et Culturelles; Grant number: SSTC-PAI P4–30; Grant sponsor: Fond National de la Recherche Scientifique; Grant number: FRFC 2.4545.96; Grant sponsor: Deutsche Forschungsgemeinschaft; Grant sponsor: Fonds der Chemischen Industrie; Grant sponsor: Patrimoine de l'Université de Liège.

*Correspondence to: Dominique Maes, ULTR, IMOL, Vrije Universiteit Brussel, Paardenstraat 65, B-1640 Sint-Genesius-Rode, Belgium. E-mail: dommaes@vub.ac.be

Received 16 March 1999; Accepted 18 June 1999

3-phosphate.[8] TIM has been the subject of extensive biophysical, enzymological, and computational studies. Each TIM monomer is formed by an eightfold repeat of a [β-strand, loop, α-helix, loop] motif. The βα-units fold up in a regular way, such that the β-strands (numbered β1 to β8) form an eight-stranded β-barrel, surrounded by the eight α-helices (numbered α1 to α8) on the outside. This folding motif is also referred to as the TIM-barrel motif. The catalytic residues are located in the β-strands and in the loops connecting the β-strands to subsequent α-helices, numbered loop 1 to loop 8 in correspondence with the numbering of the preceding β-strands. Binding of substrate or substrate analogues is accompanied by a change in conformation of loop 5, loop 6, and loop 7,[9,10] going from an open state (unliganded) into a closed state (liganded) to prevent an unwanted phosphate elimination reaction that may otherwise occur.[8] The dimer interface is formed mainly by loops 1, 2, 3, and 4; the protruding loop 3 of one subunit docks into a deep pocket between loop 1 and loop 4 of the other subunit.[11]

To date, x-ray structures of TIM have been solved (wild type and/or in complex with substrate analogues) from psychrophilic, mesophilic, thermophilic, and hyperthermophilic organisms. With respect to mesophilic organisms, the following structures have been reported: chicken (ChTIM),[12,13] yeast (YeTIM),[14] *Trypanosoma brucei* (TbTIM),[15] *Escherichia coli* (EcTIM),[16] human (HuTIM),[17] *Plasmodium falciparum* (PfTIM),[18] and *Leishmania mexicana* (LmTIM).[19] Very recently, the crystal structure of *T. cruzei* TIM[20] also has been described. The following TIM structures of extremophilic organisms have been solved: that of the thermophile Bacillus stearothermophilus (BsTIM) [21] and that of the psychrophile *Vibrio marinus* (VmTIM).[3] Here we report the structure of TIM from the hyperthermophile *Thermotoga maritima* (TmTIM). *T. maritima* belongs to one of the deepest and slowly evolving bacterial branches of the phylogenetic tree. This hyperthermophilic, strictly anaerobic, fermentative bacterium grows in the temperature range between 55° and 90°C with an optimum growth at 80°C. The N-terminus of TmTIM has been shown to be covalently linked to the C-terminus of phosphoglycerate kinase (PGK), forming a bifunctional PGK-TIM fusion protein.[22] This fusion protein is a tetramer consisting of four PGK-TIM chains. Recently, the separate TIM-enzyme has been cloned, expressed in *E. coli*, and compared with its wild-type in the PGK-TIM fusion protein. It turns out that the fusion enhances the intrinsic stability and the catalytic efficiency of TIM, but the separate TIM exhibits high intrinsic stability and can still be categorized as a hyperthermophilic enzyme.[23] In this article we also describe the results of the detailed comparison of ten TIM structures, which was aimed at finding structural determinants of thermostability.

MATERIALS AND METHODS

Expression and Purification

TmTIM was produced and purified as described previously.[23]

Sedimentation Analysis

Sedimentation velocity and sedimentation equilibrium experiments made use of a Beckman Spinco E analytical ultracentrifuge equipped with a high-sensitivity light source and a multiplexer photoelectric scanning system (AnG and AnF-Ti rotors, 12-mm double-sector cells with sapphire windows, scanning wavelength 235 and 280 nm). Before the experiments, the enzyme solutions were subjected to equilibrium dialysis against 50 mM Tris/HCl buffer pH8.6 with 2 mM EDTA. Sedimentation velocity experiments were performed at 44,000 revolutions/minute and room temperature; sedimentation coefficients were corrected for 20°C and water viscosity. For sedimentation equilibria, the meniscus-depletion technique[24] was applied to quantify possible deviations from homogeneity; experimental conditions were as follows: 15,000 and 18,000 revolutions/minute, 20.0° to 21.3°C. The quantitative evaluation was based on the linearization of the scans in ln c versus r^2 plots, with the use of a computer program provided by G. Böhm (University of Halle); for curve fitting, a monomer molecular mass of 26850 D was assumed.

Crystallization

Crystals were grown at 20°C using the hanging drop vapor diffusion technique with the aid of Hampton screening solutions. The protein solution used in the crystallization set-ups contained 8.5mg/mL protein in 70 mM TRIS HCl (pH 8.0), 2 mM EDTA, 5 mM cysteamine, and 400 mM NaCl. Drops were prepared by mixing 2.5 µl of TmTIM solution with 2.5 µl reservoir solution of 100 mM TRIS/HCl buffer (pH 8.5) with 2.0 M ammonium sulfate.

Data Collection

Crystals diffracted to 2.8 Å on a rotating anode x-ray source and data were collected at 25°C on a BigMar image plate detector mounted on an Enraf Nonius rotating anode FR571. The data were processed with DENZO.[25] Scaling, merging, and reduction of the integrated intensities was performed using SCALEPACK[25]and TRUNCATE.[26] The B-factor of the Wilson plot is 39 $Å^2$. The crystal lattice is primitive trigonal; with a = b = 125.95 Å; c=103.72 Å, and two possibilities for the space group, i.e., $P3_221$ and $P3_121$. Calculation of Matthews parameters gave a V_M of 4.4 and 2.2 $Å^3$/D for one and two dimers in the asymmetric unit, respectively.

Molecular Replacement

To find the orientation(s) of the TIM dimer in the unit cell, molecular replacement was performed with the program AMORE[27] using the crystal structure of BsTIM (1BTM; Brookhaven Protein Data Bank) as the search model. The rotation function showed one unique peak above 19 σ, while the next peak was only 7 σ. A translation was calculated for this rotation peak in both possible space groups ($P3_221$ and $P3_121$). A good translation function solution was found for space group $P3_221$. The R-factor for data between 20 and 3.5 Å for this solution dropped to 43%

after rigid body refinement. There was no indication for the presence of a second dimer in the asymmetric unit. The packing of the dimers is very loose, with large, triangular solvent channels, resulting in a crystal solvent content of more than 70%.

Refinement and Quality of the Structure

The starting model for the refinement was the BsTIM model properly positioned in the TmTIM cell. Loop 6 was deleted in both subunits, and the sequence was changed into the TmTIM sequence. Several rounds of visual inspection and improvement followed by computer refinement were done. On one hand, the model was optimized to improve its fit in a 2Fo-Fc density map with the program O[28] running on an SGI-workstation; on the other hand, refinement was pursued with a mixture of simulated annealing X-ray refinement and conventional positional and thermal factor refinement using the X-PLOR package[29] for the initial refinement calculations. For refinement, a subset of 5% of the data (the test set) was used for R-free calculations. A bulk solvent correction was applied. Electron density maps indicated a closed conformation for loop 6, which was manually rebuilt into the density. In addition, a sulfate ion was found in the active site of each subunit; its coordinates were included in the model. The final stages of the refinement were carried out with CNS;[30] water molecules were added at sites displaying a peak larger than three standard deviations above the mean in an Fo-Fc map and having a potential hydrogen-bonding partner. In total, 52 water molecules were added per dimer. The final R-factor was 21.1%, and R-free was 24.9 % for all data in a resolution range from 20 to 2.85 Å (Table I). The quality of the structure was analyzed using the programs PROCHECK[31] and WHAT IF.[32]

TABLE I. Crystallographic Data and Refinement Statistics of the TmTIM Structure

Space group	$P3_221$
Cell dimensions (Å)	125.95 125.95 103.72
Cell dimensions (°)	90 90 120
Subunits per asymmetric unit	2
V_m (Å^3/D)	4.4
Data collection statistics	
Observed reflections	88,489
Unique reflections	22,020
Overall range (Å)	20–2.85
Overall R-merge (%)	8.6
Overall completeness (%)	97.8
Last shell range (Å)	2.90–2.85
Last shell R-merge (%)	29.9
Last shell completeness (%)	90.0
B-factor from Wilson plot (Å^2)	38.7
Refinement statistics	
Protein atoms	3974
Ligand atoms	10
Solvent atoms	52
Resolution range (Å)	20.0–2.85
R-factor (%)	21.1
R-free (%)	24.9
rms bond length deviations (Å)	0.006
rms bond angle deviations (°)	1.30
$\chi_1\chi_2$ imperfection (°)[a]	31.7
rms ΔB for covalently bonded atoms (Å^2)	3.47
average B-factor, all protein atoms (Å^2)	54.7
Average B-factor, backbone atoms (Å^2)	52.9
Average B-factor, side chain atoms (Å^2)	56.6
Average B-factor, ligand atoms (Å^2)	74.4
Average B-factor, solvent atoms (Å^2)	46.2
Ramachandran plot[b]	
Most favored regions (%)	84.1
Additional allowed regions (%)	14.3
Generously allowed regions (%)	1.1
Disallowed regions (%)	0.5

[a]The $\chi_1\chi_2$ imperfection value[9] is the rms between observed $\chi_1\chi_2$ values and the nearest preferred values as found in a database of well-refined structures.
[b]As defined by PROCHECK.[31]

Structure Comparison and Sequence Alignment

The ten structures used in the comparison are found in the PDB with entry codes summarized in Table II. For the purpose of analysis, TIM structures were superimposed on the basis of the 129 C_α-atoms forming the eight framework α-helices and β-strands and using the lsq option in O.[28] The sequence alignment was made with Pileup of the GCG package[33] and checked by superimposing of the structures.

Secondary Structure Assignment

The assignment of the β-strands was done with the DSSP-software.[34] The beginnings (the N-cap positions) and the ends (the C-cap positions) of the helices were identified manually as defined by Richardson and Richardson.[35] The N- and C-caps were found by positioning an ideal helix on the TIM helix. The N-cap is the first residue of the helix for which C_α is on the ideal helical spiral, similarly the C-cap is the last residue on the helical spiral.

Volumes, Cavities and B-Factors

Molecular volumes were calculated with the MSP software.[36] Atomic radii were as described previously.[13] Cavities of which more than 70% of the surface is hydrophobic are classified as hydrophobic cavities. Carbon and sulfur atoms are considered hydrophobic, whereas nitrogen and oxygen atoms are considered hydrophilic.

Hydrophobicity

The accessible surface area and the difference in accessible surface area upon protein folding and assembly were calculated with the NACCESS software[37] using a probe radius of 1.4 Å. For the unfolded state, accessibility was calculated using an extended Ala-X-Ala peptide. Carbon and sulfur atoms are considered hydrophobic, whereas nitrogen and oxygen atoms are considered hydrophilic.

Hydrogen Bonds and Salt Bridges

Hydrogen bonds between protein atoms were calculated for all proteins using the HBPLUS routine[38] with the default parameters for distances and angles. When two

TABLE II. The TIM PDB Files Used in the Structure Comparison

Organism	Code	Temperature range	PDB code	Resolution (Å)	Asymmetric unit	Conformation of active site loops		Reference
						Subunit A	Subunit B	
V. marinus	Vm	Psychrophile	1AW1	2.7	4 dimers	Closed	Closed	3
T. brucei	Tb	Mesophile	5TIM	1.8	Dimer	Open	Almost closed	15
L. mexicana	Lm	Mesophile	1AMK	1.8	Monomer	Closed	Closed	19
P. falciparum	Pf	Mesophile	1YDV	2.2	Dimer	Open	Open	18
Human	Hu	Mesophile	1HTI	2.8	Dimer	Open	Closed	17
Chicken	Ch	Mesophile	8TIM	2.5	Dimer	Open	Open	12, 13
Yeast	Ye	Mesophile	7TIM	1.9	Dimer	Closed	Closed	14
E. coli	Ec	Mesophile	1TRE	2.6	Dimer	Open	Open	16
B. stearothermophilus	Bs	Thermophile	1BTM	2.8	Dimer	Closed	Closed	21
T. maritima	Tm	Hyperthermophile	1B9B	2.8	Dimer	Closed	Closed	

atoms of opposite charge were observed to be within 4 Å, they were assigned to a salt bridge. Barlow and Thornton[39] recommended this distance threshold after extensive analysis of several protein structures. Positively charged atoms included side-chain nitrogens in Lys and Arg, whereas negatively charged atoms are the side-chain oxygens of Asp and Glu. Salt-bridge networks consist of three or more salt-bridged residues.

Charge Distribution at N- and C-Terminal Ends of Helices

For this analysis only the framework helices were used, except for the C-terminal end of helix 8, which is not well-defined. The center point of the N-terminal end of the helix is calculated from the coordinates of the main chain C_α, N and C atoms of the N-cap, N-cap +1, N-cap +2, and N-cap +3 residues, belonging to the first turn of the helix. In an analogous way the center point of the C-terminal end was calculated, using the C-cap-3, C-cap-2, C-cap-1, and C-cap residues. All charged atoms within a distance of 7 Å of this center were calculated. Positively charged atoms included side-chain nitrogens in Lys and Arg, with a net contribution of +1 and +1/3, respectively for each nitrogen atom, whereas negatively charged atoms concern the side-chain oxygens of Asp and Glu, with a net negative charge of −½ for each oxygen atom. The average charge at the N-terminal end of a helix is calculated by first summing all charges within the defined spheres of all the available helices then dividing by the number of helices. The average charge at the C-terminal is calculated the same way.

RESULTS AND DISCUSSION

TmTIM X-Ray Structure

The structure of *T. maritima* TIM has been refined at 2.85 Å resolution to a model with good geometry and crystallographic quality (Table I). In this crystal form there is one TmTIM dimer per asymmetric unit: the model for the TmTIM dimer consists of residues 2–253 for subunit A and residues 1– 255 for subunit B. There was no clear density for the N- and C-terminus of the first subunit. The residue-stretch composed of residues 33 to 36 in both subunits as well as loop 6 in subunit B display high thermal B-factors; nevertheless, density was visible in the omit map, and the coordinates were incorporated in the structure. The stereochemical quality of the structure was analyzed with the program PROCHECK.[31] The Ramachandran plot shows only two outliers, concerning the Lys13 residue of both subunits, which are in a strained conformation in each TIM structure. All stereochemical parameters for the main chain and side-chain atoms are better than those for proteins refined to a similar resolution. The thermal B-factors of the complete structure are high with an average of 52.9, 56.6, and 54.7 $Å^2$ for main chain, side-chain, and all protein atoms, respectively. The high average B-value agrees with the high B-factor of the Wilson plot (Table I) and correlates with the high solvent content of the crystal. Loops 5, 6, and 7 are in the closed conformation in both subunits. A sulfate ion occupies the active site of both subunits (with an average thermal B-factor of 74.4 $Å^2$). Fifty-two waters were included in the structure with an average B-factor of 46.2 $Å^2$. The packing of the TIM dimers is very loose with triangular solvent channels with a diameter of 89 Å. The TmTIM structure is very similar to all other TIM structures with a Cα rmsd for the framework residues ranging from 0.8 to 1.4 Å (Table III). Both subunits are very similar with a Cα rmsd of 0.5 Å for all main chain atoms.

Tetramerization

The crystallographic twofold axis perpendicular to the threefold screw axis rotates the TIM dimer in such a way that a dimer of dimers with tetrahedral symmetry is formed. Figure 1**A** shows the tetrameric organization of TmTIM. The noncrystallographic twofold axis ($\kappa = 179.5°$) of the canonical dimer is perpendicular to the crystallographic twofold, resulting in the near 222 symmetry. The dimer of dimers is stabilized by hydrophobic and polar interactions of residues in loop 5 and helix 5. The major interdimeric contacts consist of two disulfide bridges between the Cys142 of each monomer and its symmetry equivalent. Furthermore, there is a hydrophobic contact because of Leu139, a salt link between Glu150 and Lys137, and some hydrogen bonds, shown in detail in Figure 1**B**. Because of the twofold symmetry, the latter contacts are found twice, on either side of the disulfide bridge. The salt bridges each belong to a salt-bridge network involving

TABLE III. Structural and Sequence Comparison

	Vm	Tb	Lm	Pf	Hu	Ch	Ye	Ec	Bs	Tm
Vm	100	38.9	39.3	39.4	41.6	41.2	43.1	65.7	41.3	39.9
	0.23	0.98	0.91	1.13	0.86	0.84	0.81	0.58	1.13	0.92
	0.25	1.41	1.29	1.57	1.42	1.33	1.27	0.60	1.53	1.13
Tb	38.9	100	69.6	43.1	52.6	52.0	49.2	42.9	40.7	42.2
	0.98	0.26	0.42	0.79	0.85	0.79	1.03	0.90	1.27	1.23
	1.41	0.26	0.46	1.23	1.18	1.12	1.26	1.36	1.44	1.40
Lm	39.3	69.6	100	45.5	50.6	50.4	45.9	42.5	43.5	42.2
	0.91	0.42	0.0	0.72	0.90	0.81	0.99	0.86	1.29	1.22
	1.29	0.46	0.0	1.20	1.19	1.12	1.19	1.27	1.46	1.37
Pf	39.4	43.1	45.5	100	42.5	43.3	41.5	40.2	38.1	40.7
	1.13	0.79	0.72	0.27	1.11	1.08	1.26	1.02	1.46	1.37
	1.57	1.23	1.20	0.37	1.24	1.19	1.45	1.54	1.53	1.57
Hu	41.6	52.6	50.6	42.5	100	89.1	53.3	44.9	39.0	41.7
	0.86	0.85	0.90	1.11	0.44	0.42	0.80	0.88	1.15	1.05
	1.42	1.18	1.19	1.24	0.46	0.50	0.99	1.45	1.42	1.40
Ch	41.2	52.0	50.4	43.3	89.1	100	53.3	45.3	40.2	43.3
	0.84	0.79	0.81	1.08	0.42	0.35	0.72	0.82	1.11	0.99
	1.33	1.12	1.12	1.19	0.50	0.36	0.86	1.35	1.41	1.35
Ye	43.1	49.2	45.9	41.5	53.3	53.3	100	45.1	37.9	42.1
	0.81	1.03	0.99	1.26	0.80	0.72	0.24	0.85	1.39	1.06
	1.27	1.26	1.19	1.45	0.99	0.86	0.26	1.32	1.81	1.46
Ec	65.7	42.9	42.5	40.2	44.9	45.3	45.1	100	39.7	42.7
	0.58	0.90	0.86	1.02	0.88	0.82	0.85	0.39	1.11	0.94
	0.60	1.36	1.27	1.54	1.45	1.35	1.32	0.41	1.52	1.10
Bs	41.3	40.7	43.5	38.1	39.0	40.2	37.9	39.7	100	50.0
	1.13	1.27	1.29	1.46	1.15	1.11	1.39	1.11	0.27	0.83
	1.53	1.44	1.46	1.53	1.42	1.41	1.81	1.52	0.28	1.09
Tm	39.9	42.2	42.2	40.7	41.7	43.3	42.1	42.7	50.0	100
	0.92	1.23	1.22	1.37	1.05	0.99	1.06	0.94	0.83	0.30
	1.13	1.40	1.37	1.57	1.40	1.35	1.46	1.10	1.09	0.30

The numbers in each block refer to: % sequence identity after alignment (calculated from the sequence alignment shown in Fig. 3), rmsd of framework C-atoms (129 atoms) (subunit A), and rmsd of all equivalent C-atoms after alignment (subunit A), excluding loops 5, 6, and 7, which are known to adopt different conformations in the presence or absence of ligand[9] and excluding insertions/deletions (including one residue before and after). On the diagonal the same quantities are given for subunit A on subunit B of the same species.

Glu133 and Lys137 of one subunit, connected to Glu150, Lys146, and Asp107 of the other subunit. This new contact area buries 537 Å^2 of accessible surface area (ASA) (per monomer), of which 69% is hydrophobic. These values have to be compared with 1,758 Å^2 (per monomer), of which 70% is hydrophobic, buried between the monomers in the "canonical dimer."

The tetrameric assembly is also confirmed by analytical ultracentrifugation (AUC) studies (Table IV). The results of sedimentation velocity experiments in the absence and in the presence of cysteamine resulted in s-values around 5.4 S, corresponding to a molecular mass of globular proteins between 90 and 100 kD.[40] Sedimentation equilibrium experiments were fitted, taking into account the calculated partial specific volume of the native enzyme ($V_p = 0.750$ cm^{3}g^{-1}) on the one hand and tentative values for the partial volume and the density in the presence of 6 M GdmCl ($V_p' = 0.740$ cm^3 g^{-1}, $\rho' = 1.145$ g cm^{-3}) on the other hand. The latter value for V_p is based on model studies using bovine serum albumine as a standard;[41] whether this is appropriate for proteins without intramolecular cystine cross-links is unclear. Because the boyancy term causes a large range of error at high solvent densities, M_W in the presence of 6M GdmCl may be too high by a factor of ≤ 2. The results in dilute buffer in the absence and in the presence of reducing agent clearly show that in vitro TmTIM forms a tetramer (Table IV).

The TmTIM structure also indicates a mode of assembly for the tetrameric PGK-TIM fusion protein. In the TmTIM tetramer (Figure 1A) the N-termini of each subunit are solvent exposed. This suggests that in the wild-type fusion protein the TmTIM tetramer forms the core and each TmTIM subunit is covalently linked at its N-terminus to the C-terminus of a PGK unit.

Two other hyperthermophilic archaeal TIMs were reported to exist also in a tetrameric form.[42,43] Also, various other enzymes from thermophilic and hyperthermophilic enzymes are known to exist as higher-order association states compared with their mesophilic analogues, suggesting that the formation of higher-order oligomers is one way by which hyperthermostability is achieved in nature.[1]

Conserved Salt Bridge

The sequences of the ten TIM structures are tabulated in Figure 2. The fully conserved residues are all, except one, near the active site pocket. The conservation of these

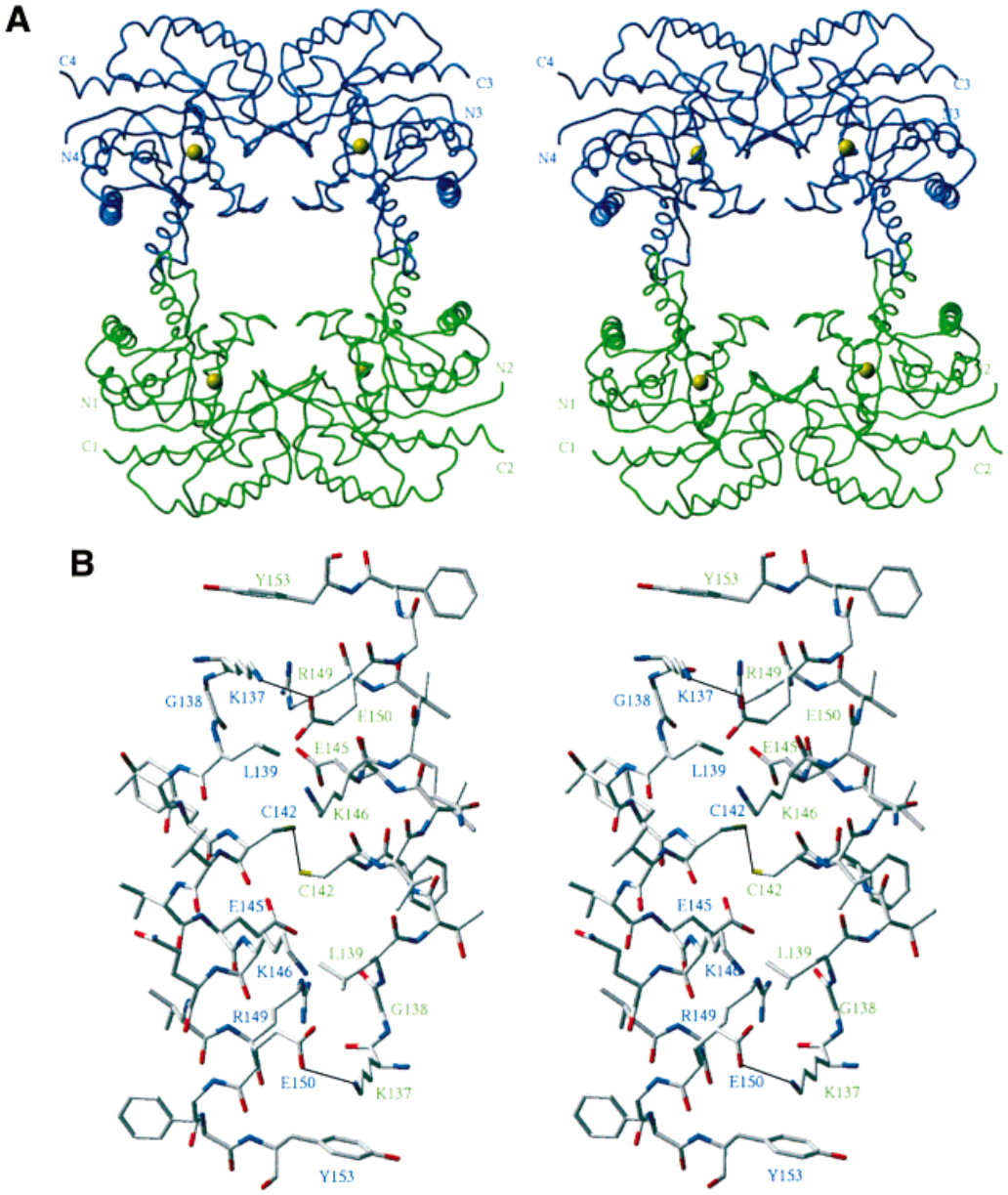

Fig. 1. **A**: Stereo view of the C_α-trace of the TmTIM tetramer, composed of two canonical dimers (blue and green), related by a crystallographic twofold axis. The contacts between the two canonical dimers are between residues of loop 5 and helix 5. The N- and C-termini of each subunit are indicated with N1, C1, N2, C2, N3, C3, N4, and C4. The active sites are marked by yellow spheres. **B**: Stereo view of the interdimeric interface. The labeled residues are involved in interdimeric contacts. Each residue label has the same color as the corresponding subunit in Figure 1A.

residues is therefore correlated with the architecture of the catalytic site. The only exception is the conserved arginine at position 192. This arginine is located at the other end of the TIM barrel and is involved in a conserved salt bridge with Asp230 and/or Asp228 (Fig. 3). This salt bridge anchors the C-terminal ends of helix 6 and helix 7 to each other, and this anchoring is completely conserved in all available structures. Although the location of this interaction is at a distance of 20 Å from the active site, the strict conservation of this salt bridge points to an important function. The importance of this anchoring interaction might be related to the conformational flexibility of loop 6 and loop 7, located at the N-terminal ends of helix 6 and helix 7, respectively, which is crucial for the catalytic properties of TIM.[9]

Comparative Analysis

Which structural features can be correlated with the differences in environmental temperature in the TIM family? If all TIMs would use the same mechanism of thermal adaptation, a trend would be visible; in this case the relevant variable(s) would increase or decrease in going from a psychrophilic TIM to a hyperthermophilic TIM. However, it is also possible that different approaches

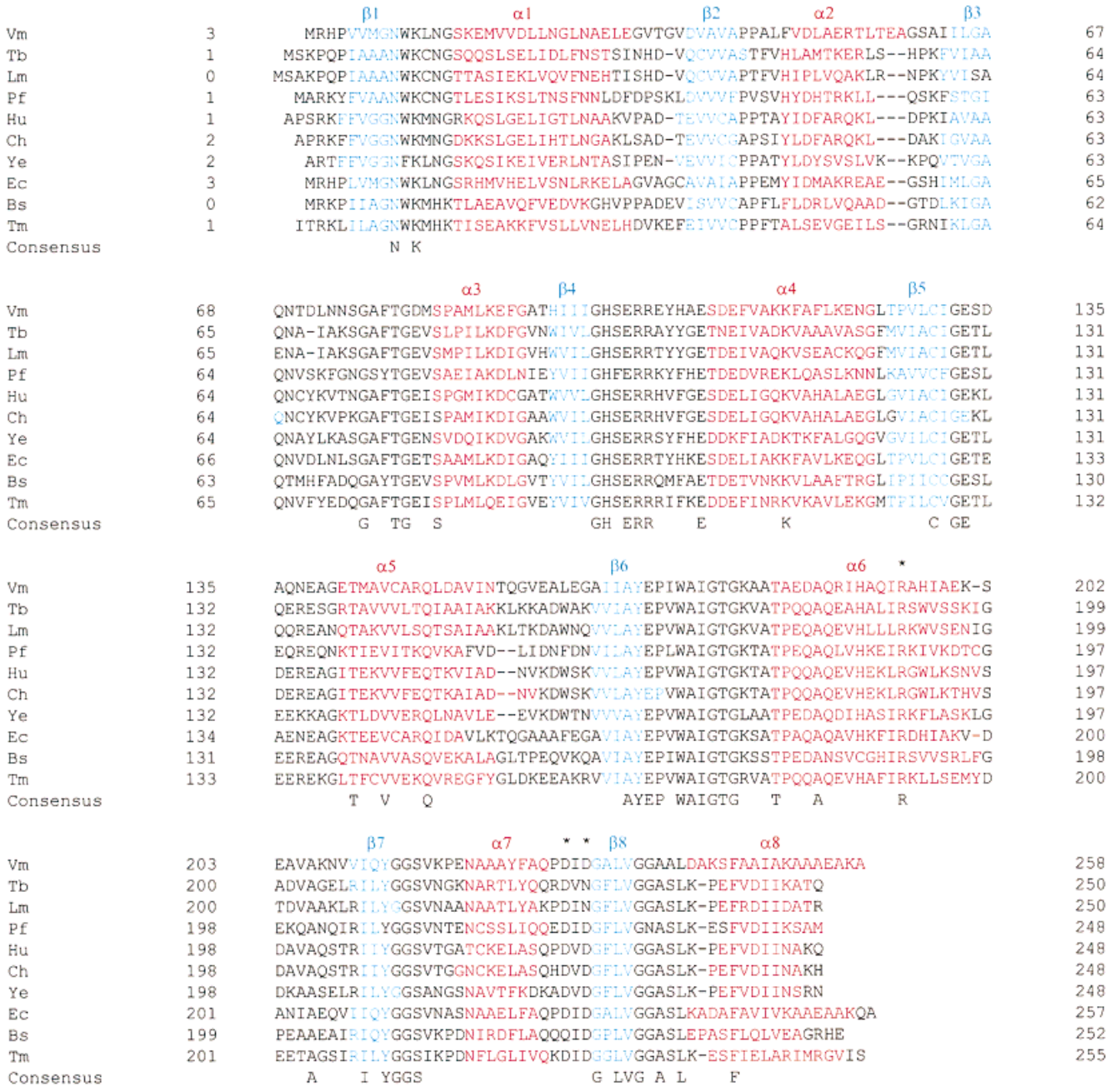

Fig. 2. Sequence alignment of the ten TIMs. The β-strands (blue) and the α-helices (red) are labeled β1 to β8 and α1 to α8, respectively. The conserved residues in these ten TIMs are shown on the "Consensus" line. The residues involved in the conserved salt bridge (Fig. 3) are indicated by an asterisk.

are being used to adapt to psychrophilic conditions and thermophilic conditions; in this case, unique properties for psychrophilic and thermophilic enzymes should become apparent. The thermal stability of mesophilic proteins is only marginal; in the range of 10 to 15 kcal/mol.[6] Hence, the addition or deletion of a few well chosen, weak interactions is sufficient to convert a mesophilic enzyme into a thermostable enzyme.[19,44,45] It seems, therefore, likely that for ultrastable wild-type proteins also small adjustments can contribute significantly to the adaptation toward extremes of environmental temperature. Unfortunately, such specific adaptations may not be detectable when systematic comparisons of TIMs from different species are done because there are just too many exchanges.[46] Extremophilic enzymes not only have optimal stability but also must fold, assemble, and function at the extreme temperatures of their environment. Therefore, some unique features of the sequences or structures of these enzymes might, in fact, be adaptations required for optimal folding and function but not for optimal stability.

TABLE IV. Results of Analytical Ultracentrifugation Experiments With TmTIM in 50 mM Tris pH 8.6, 2 mM EDTA

Conditions	S-value (S)	M_W (D)	Correlation coefficient[a]
Buffer, no cysteamine	5.43 ± 0.15	103,827 ± 3,065	0.9999
Buffer, 5 mM cysteamine	5.31 ± 0.15	108,753 ± 6,796	0.9995
Buffer, 6 M GdmCl, 5 mM cysteamine	nd[b]	102,321 ± 9,127	0.9994

[a]The given correlation coefficients refer to the quality of the ln c vs r^2 linearization. The true range of error in M_W in dilute buffer amounts to approximately 5%.
[b]Value not determined.

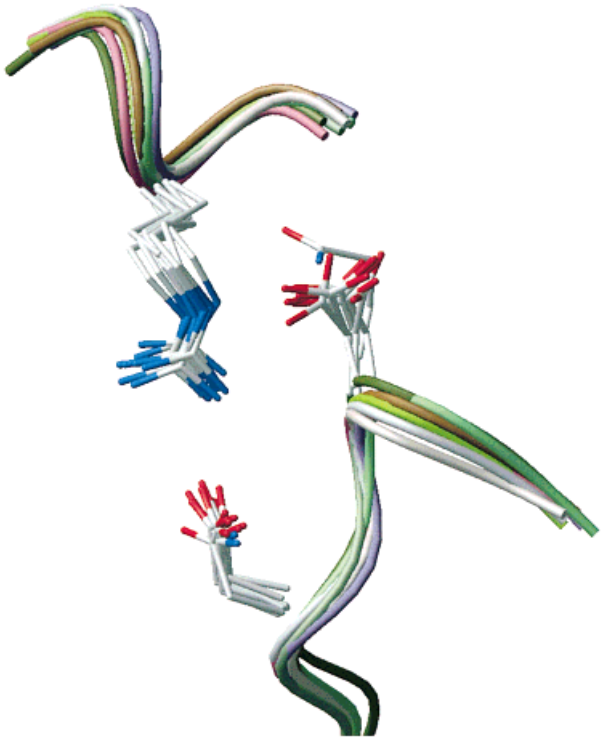

Fig. 3. The conserved salt bridge between the C-terminal ends of helix 6 and helix 7 for the ten TIM structures. The side-chains of Arg192, Asp228, and Asp230 of TmTIM and their equivalents in the other structures are shown explicitly. The main chain of the ten structures are shown in different colors.

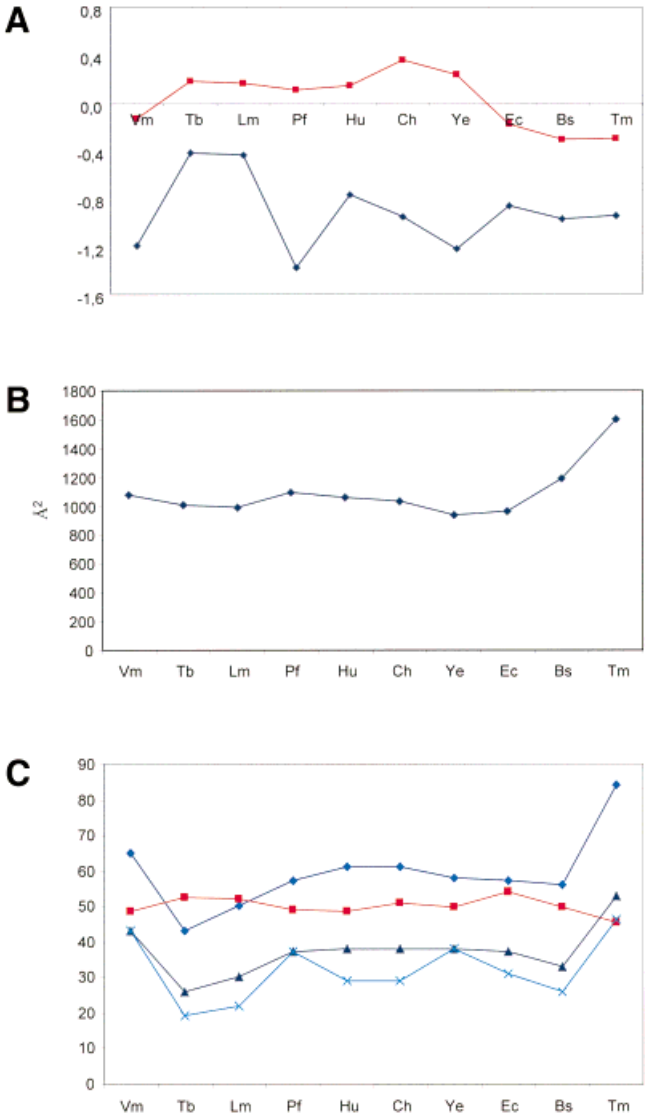

Fig. 4. Graphs displaying various parameters for each of the ten TIM structures. The horizontal axis displays the ten TIMs with increasing thermal stability. **A**: Average charge within a sphere of 7 A at the N-terminal ends (♦) and C-terminal ends (■) of the framework helices. **B**: Hydrophobic ΔASA of the folded monomer buried on assembly (Å²) (see also Table VII). **C**: Number of hydrogen bonds (:10) (■), number of salt bridges (▲), number of residues in salt bridges (♦), and number of residues in salt bridge networks (**x**) (the numbers have been normalized per dimer).

The ten different structures used for the comparison are summarized in Table II; their sequence alignment is depicted in Figure 2. The secondary structure of the framework β-strands and α-helices is also shown; the start and end of these secondary structural elements for the different species vary. The percentage sequence identity is given in Table III. The TIM sequences are highly conserved, despite the wide range of species included in the comparison. The lowest sequence identity (38%) is found for the comparison of BsTIM and YeTIM; the highest sequence identity (89%) is between ChTIM and HuTIM. VmTIM and EcTIM have a high sequence identity (66%); the peculiar structural features of VmTIM also occur in EcTIM.[3] TmTIM has the highest sequence identity (50%) with BsTIM; both are thermostable. A good correlation exists between the percentage sequence identity and the C_α rmsd for the superimposed framework residues. For the comparisons with low sequence identity (less than 40%), the rms is near 1.4 Å, and for the comparisons with high sequence identity (70% to 90%), the rms value is between 0.3 and 0.4 Å.

Sequences

Previous studies have attempted to correlate amino acid compositions and sequence alignments with thermal stability.[47] Table V lists the amino acid composition of the ten TIM structures. The largest deviation from the average is the high alanine content of VmTIM (48 of 256 residues). This seems to be a property of the phylogenetic family, because EcTIM also has a high (45 of 255 residues) alanine content. Consequently, for both TIMs, the alanine content of the framework helices is also high (27 in VmTIM and 22 in EcTIM) (Table VI). This high alanine content in the helices of VmTIM and the low content in TmTIM is surprising because alanine is known to stabilize helices.[48] The glycine and proline content, affecting the flexibility of the unfolded state as well as the content of thermolabile residues (e.g., Cys, Asn, and Gln),[49] cannot be correlated with thermal stability. The slightly deviating content of some residues in TmTIM, like the high percentage of charged residues (28%) compensated by a low percentage of polar residues (16%), is not found in the thermophilic BsTIM; the opposite feature is also not found in VmTIM. Hence, it seems that the discrimination between psychrophilic, mesophilic, and (hyper)thermophilic TIMs cannot be correlated with well-defined shifts in specific amino acid compositions.

Secondary structure

The only sound basis for the discussion of extremophilic adaptation is the 3D structure, permitting the forces underlying protein stability under extremes of physical conditions to be defined in an unambiguous way. α-Helices and extended β-sheet structures contribute significantly to protein stability; loops in thermostable enzymes have sometimes been observed to be shorter than those in their mesophilic counterparts, thus stabilizing the folded or destabilizing the unfolded state. In the case of the ten different TIM structures, no substantial differences can be detected regarding the fraction of amino acids involved in secondary structure, taking into account also the helical arrangement in some of the loops connecting the framework helices and strands.

Recent studies[50,51] independently concluded that enhanced stabilization of helices is a necessary, but not a sufficient, condition for protein thermostability. Two types of contributions were distinguished: (a) "intrinsic helical propensities," associated with the loss of conformational entropy of amino acid residues in helical arrangements, and (b) specific amino acid patterns at the helical ends. As far as the first of these two is concerned, it was found that the helices of thermophilic proteins contain a lower percentage of β-branched residues (i.e., Val, Ile, and Thr) compared with their mesophilic equivalents. The rotameric conformations of these residues are constrained by the helical conformation. Table VI shows the amino acid composition of the framework α-helices (in absolute values and normalized values); all mesophilic sequences are grouped together. The only striking feature is the high alanine content of the VmTIM helices and the low alanine content of the TmTIM helices, as discussed earlier. Summation of the contents of β-branched residues gives normalized values of 0.7, 1.2, 1.1, and 1.1 for psychrophilic, mesophilic, thermophilic. and hyperthermophilic TIMs, respectively. Hence, a higher percentage of these residues is not present in the (hyper)thermophilic TIMs, but the opposite is true for the psychrophilic TIM. In regard to the earlier mentioned point (b), helix-stabilizing factors have also been identified for the N- and C-capping boxes.[35,51] We analyzed the amino acid compositions at the N-cap and C-cap positions and their neighborhood ($N-4 => N+4$ and $C+4 => C-4$): no significant differences in preference were found between the mesophiles and the extremophiles (data not shown). This analysis is unfortunately hampered by the availability of only one psychrophilic, thermophilic, and hyperthermophilic structure, which prevents a reliable statistical study.

Interactions of charged and polar groups with the helix macrodipole can increase the stability of a protein.[52,53] Therefore we analyzed the charge distribution at the N-terminus and C-terminus of the framework α-helices. For this, the presence of charged side-chain atoms within a sphere of 7 Å from the N- and C-cap of these helices was calculated (Fig. 4**A**). The analysis shows that this charge distribution is not different in the psychrophilic and thermophilic enzymes. The analysis also indicates that a remarkable favorable charge preference is present at the N-terminus but not at the C-terminus.

Volumes, cavities, and B-factors

As reviewed by Lee et al.,[54] variation of cavity volumes and compactness contribute to optimal stability at different ambient temperatures. The molecular volumes and the cavity volumes for the ten TIMs are summarized in Table VII. The total cavity volume varies between 0.6% and 1.2% of the volume of the protein itself. The substantial variations of the cavity volumes within the mesophilic family as well as in the complete set of the ten TIM structures makes it unlikely that cavities play a critical role in the stabilization of the enzyme. Analysis of the size of predominantly hydrophobic cavities shows no correlation with thermal stability. The compactness, calculated as the average volume occupied by each atom, also is not related to thermal stability.

The dynamic properties of the TIM-structures were analyzed by comparing the B-factor distribution for each structure. Such B-factor distribution will also be influenced by solvent content and the packing of the crystal, which vary significantly for these structures. The mean B-factors as well as the distributions of the B-factor (expressed as the rmsd with respect to the mean) were calculated. A broad range of values was obtained, which did not correlate with the thermal stability.

Hydrophobic interactions

The importance of the hydrophobic effect on protein folding and stability is generally accepted.[55] Because the correct analytical solution for this interaction is complex, a simplification based on accessible surface calculations is

TABLE V. Total Amino Acid Composition

	Vm	Tb	Lm	Pf	Hu	Ch	Ye	Ec	Bs	Tm
A-Ala	48	34	33	15	28	28	25	45	29	15
C-Cys	2	3	4	4	5	4	2	3	4	3
D-Asp	12	8	8	14	12	13	15	10	12	9
E-Glu	22	13	15	19	17	17	17	21	20	29
F-Phe	8	8	6	13	8	8	11	6	9	12
G-Gly	23	19	16	14	25	27	22	22	22	24
H-His	6	5	6	5	4	8	3	8	6	4
I-Ile	17	19	19	19	15	17	15	19	16	23
K-Lys	13	17	17	22	20	22	21	16	12	19
L-Leu	18	17	17	19	15	17	19	17	19	23
M-Met	6	3	3	2	2	2	0	7	5	5
N-Asn	12	10	11	17	8	7	12	9	5	6
P-Pro	8	7	10	4	10	7	7	7	13	7
Q-Gln	8	13	13	12	11	9	7	11	14	8
R-Arg	7	9	8	8	8	7	8	8	11	14
S-Ser	10	18	13	18	12	12	16	11	13	12
T-Thr	11	12	16	13	14	11	12	9	12	10
V-Val	19	25	25	21	25	22	26	19	25	24
W-Trp	2	5	5	2	5	5	3	2	2	2
Y-Tyr	4	5	6	7	4	4	6	5	4	6
Total	256	250	251	248	248	247	247	255	253	255
% Charged	21.1	18.8	19.1	25.4	23.0	23.9	24.7	21.6	21.7	27.8
% Polar	18.4	23.2	23.5	26.2	19.8	19.0	20.2	18.8	19.8	15.7
% Apolar	51.6	50.4	51.0	42.7	47.2	46.2	46.2	51.0	49.8	47.1
% Glycines	9.0	7.6	6.4	5.6	10.1	10.9	8.9	8.6	8.7	9.4
Charge	−14	+5	+2	−3	−1	−1	−3	−7	−9	−5

TABLE VI. Amino Acid Composition of the Framework Helices

	Number of residues				Normalized preferences[a]			
	Vm	Mesophilic[b]	Bs	Tm	Vm	Mesophilic[b]	Bs	Tm
A-Ala	27	86	14	6	2.73	1.42	1.59	0.64
C-Cys	1	7	1	1	0.55	0.62	0.61	0.57
D-Asp	6	41	7	2	0.93	1.03	1.21	0.32
E-Glu	12	54	7	13	1.66	1.22	1.08	1.88
F-Phe	7	22	6	7	1.60	0.82	1.54	1.67
G-Gly	4	22	3	6	0.45	0.40	0.38	0.71
H-His	2	19	1	2	0.82	1.27	0.46	0.86
I-Ile	5	57	2	8	0.86	1.59	0.38	1.44
K-Lys	8	66	5	7	1.04	1.40	0.73	0.96
L-Leu	9	60	11	14	0.97	1.05	1.33	1.58
M-Met	3	8	1	3	1.28	0.55	0.48	1.34
N-Asn	5	26	4	3	1.01	0.85	0.90	0.63
P-Pro	1	13	3	2	0.20	0.42	0.66	0.41
Q-Gln	4	43	5	6	0.91	1.58	1.27	1.42
R-Arg	4	21	5	5	0.74	0.63	1.03	0.96
S-Ser	4	43	6	7	0.54	0.94	0.91	0.99
T-Thr	4	41	6	3	0.61	1.01	1.02	0.48
V-Val	6	53	14	11	0.76	1.09	1.98	1.45
W-Trp	0	4	0	0	0.00	0.49	0.00	0.00
Y-Tyr	1	8	0	2	0.27	0.35	0.00	0.56
Totals	113	694	101	108				

[a]The normalization used the natural occurrences in percentage, as calculated by Nakashima et al.[65] (A: 8.74; C: 1.62; D: 5.72; E: 6.39; F: 3.87; G: 7.82; H: 2.15; I: 5.15; K: 6.78; L: 8.20; M: 2.08; N: 4.39; P: 4.49; Q: 3.19; R: 4.81; S: 6.56; T: 5.84; V: 7.01; W: 1.17; Y: 3.33).
[b]The mesophilic TIMs are grouped together.

used.[56,57] Three different comparisons of hydrophobic surfaces are given in Table VII. First, the hydrophobicity of the protein envelope is calculated: no significant differences related to thermostability are observed when the ten different TIM structures are compared. Second, values for the total accessible surface area (ΔASA) and the hydrophobic ΔASA, buried when the unfolded chain is folded into the monomer structure, were calculated.[58] The burial of hydrophobic surface area shows its maximum value for BsTIM and TmTIM: for TmTIM 17,378 Å^2 of hydrophobic ΔASA is buried upon monomer folding. For BsTIM it is 584 Å^2 (3%), and for TmTIM it is 1,363 Å^2 (8%) more compared with VmTIM. It is interesting to note that the amount of buried hydrophobic area is a constant fraction of the total ΔASA buried upon folding (varying between 59.0% and 59.7%), in agreement with previous studies.[59] Third, the total ΔASA and hydrophobic ΔASA buried on assembly of the folded monomers into oligomers was calculated per monomer. These values are much higher for both thermophiles; for TmTIM 1,599 Å^2 is buried (per monomer) on assembly. For BsTIM it is 117 Å^2 (7%), and for TmTIM it is 528 Å^2 (50%) more compared with VmTIM. The large increase seen for TmTIM (Fig. 4**B**) is largely because of the formation of the tetramer. The buried ΔASA on assembly has the highest percentage of hydrophobicity for both thermophilic TIMs (67.8% and 69.7%). These hydrophobicity calculations confirm the proposal that the hydrophobic term makes a major contribution to the enhanced stability of thermostable TIMs.[21] For TmTIM the increase of buried hydrophobicity is achieved at three levels: upon folding the

TABLE VII. Volumes, Cavities, ΔASA, and Hydrophobicity

	Vm	Tb	Lm	Pf	Hu	Ch	Ye	Ec	Bs	Tm
Molecular volume of the oligomer (Å^3)	65473	66800	67378	70203	65805	65012	65723	65522	65346	141695
Total volume of cavities in the oligomer (Å^3)	374	773	589	535	616	656	544	409	453	1594
Total volume of the hydrophobic cavities in the oligomer (Å^3)	204	287	248	206	308	425	216	287	252	896
Total number of structured atoms in the oligomer	3733	3766	3812	3914	3736	3734	3766	3772	3765	7948
Compactness[a] (Å^3)	17.44	17.53	17.52	17.80	17.45	17.24	17.31	17.26	17.24	17.63
Total ASA of the folded oligomer (Å^2)	18586	19198	19230	20378	18725	19623	19017	19510	17671	37073
Hydrophobic ASA of the folded oligomer (Å^2)	10693	11304	11573	10455	10873	11330	10787	11430	9993	21050
% Hydrophobicity[b]	57.5	58.9	60.2	51.3	58.1	57.7	56.7	58.6	56.5	56.8
Total ΔASA buried on folding of the monomer (Å^2)	27060	27376	27683	27569	26844	26378	26960	27165	28006	29457
Hydrophobic ΔASA buried on folding of the monomer (Å^2)	16015	16148	16322	16258	15867	15650	16093	16043	16599	17378
% Hydrophobicity[c]	59.2	59.0	59.0	59.0	59.1	59.3	59.7	59.1	59.3	59.0
Total ΔASA of the folded monomer buried on assembly (Å^2)	1663	1533	1477	1648	1686	1603	1622	1635	1752	2295[e]
Hydrophobic ΔASA of the folded monomer buried on assembly (Å^2)	1071	1003	989	1092	1058	1032	932	965	1188	1599[f]
% Hydrophobicity[d]	64.4	65.5	66.9	66.2	62.8	64.4	57.4	59.0	67.8	69.7

[a]Compactness = molecular volume (excluding the cavity volumes) of the oligomer/total number of structured atoms in the oligomer.
[b]% Hydrophobicity = (hydrophobic ASA of the oligomer/total ASA of the oligomer) · 100%.
[c]% Hydrophobicity = (hydrophobic ΔASA buried on folding of the monomer/total ΔASA buried on folding of the monomer) · 100%.
[d]% Hydrophobicity = (hydrophobic ΔASA of the folded monomer buried on assembly/total ΔASA of the folded monomer buried on assembly) · 100%.
[e]1758 Å^2 at the canonical monomer-monomer interface, 537 Å^2 at the new dimer-dimer interface.
[f]1229 Å^2 at the canonical monomer-monomer interface, 370 Å^2 at the new dimer-dimer interface.

monomer, in the canonical monomer-monomer interface, and in the new dimer-dimer interface (Table VII).

Polar interactions

For some thermostable proteins a correlation between thermostability and the number of hydrogen bonds has been reported.[60] The respective numbers for the ten TIM structures, presented in Figure 4**C**, turn out to be closely similar; no general trend related to thermostability can be observed. Also splitting up the total number of H-bonds into main chain–main chain, main chain–side-chain and side-chain–side-chain interactions does not allow significant differences to be detected (data not shown).

Finally, salt bridges and salt-bridge networks have been proposed to play a key role in the maintenance of enzyme stability at high temperatures.[61–63] The number of salt bridges and the number of residues involved, as well as the number of residues involved in salt-bridge networks, are presented in Figure 4**C**. Superstable TmTIM has the highest number of salt bridges (0.11 per residue), which is much higher than the average observed in mesophilic TIMs (0.07 per residue). In other superstable proteins, a value of 0.11 salt bridges per residue has been found, compared with 0.06 salt bridges per residue in the mesophilic homologues.[63] In thermostable BsTIM no increase in salt bridges is observed. However, also in psychrophilic VmTIM a high number of salt bridges is present (0.09 per residue). An increase in salt bridges was also observed in psychrophilic citrate synthase,[2] but not in psychrophilic α-amylase.[4] It has been speculated that the increase of salt bridges in psychrophilic citrate synthase could be important for preventing cold denaturation.

The higher number of residues involved in salt-bridge networks in TmTIM is mainly due to the four intersubunit networks in the new dimer-dimer interfaces. The existence of these networks corroborates the observation that extensive intersubunit salt bridge networks play a major role in the stabilization of multisubunit enzymes.[64]

CONCLUSIONS

The stability of a protein is determined by the enthalpic and entropic terms of the free energy difference (ΔG) between the folded state and the unfolded state. The marginal stability of proteins depends on favorable electrostatic and hydrophobic interactions. The temperature dependence of these interactions is complex. It is poorly

understood how the adaptation of protein stability to ambient temperatures came about during evolution. From the marginal differences in ΔG we know that small adjustments are sufficient to achieve this goal. Some of these adjustments follow an average trend and some are adaptations unique for the particular structure. To address this question we have solved the crystal structure of a superstable TIM and compared ten TIM crystal structures, including representatives adapted to both the lower and upper temperature limits of life.

The TmTIM structure stands out from the mesophilic TIM structures, possessing more salt bridges and more buried hydrophobicity upon both folding and assembly. The importance of these two interactions for superstability is supported by the observation that at the extra interface in the tetramer, both extra salt bridges and a significant amount of buried hydrophobicity are observed.

The comparative analysis of the ten TIM structures did not indicate a common adaptive mechanism for the complete temperature scale. It was found that in psychrophilic TIM and hyperthermophilic TIM salt-bridge interactions are increased compared with interactions in mesophilic TIMs. With respect to adaptation at high temperature, it is obvious that in both *B. stearothermophilus* and *T. maritima* TIM, a change of the distribution of hydrophobic residues is detectable, such that in the thermophilic TIMs more hydrophobicity is buried inside the folded and assembled protein. In *T. maritima* TIM, as in some other thermophilic proteins, this effect is among others achieved by changing the quaternary structure to a higher state of association.

ACKNOWLEDGMENTS

D.M. is a research associate of the Belgian National Science Foundation (FWO). She thanks the EMBL in Heidelberg, where part of this work was carried out. In the context of this study TmTIM data were also collected at the EMBL X11 beamline at the DORIS storage ring, Desy, Hamburg. Dr. Artymiuk and Dr. Murthy kindly made available to us the coordinates of the refined chicken and malaria TIM structure, respectively, before deposition at the Brookhaven database. The TmTIM x-ray coordinates were submitted at the Brookhaven database and have entry code 1B9B. M.A. acknowledges grants from the Actions de Recherche Concertées, the Services Fédéreaux des Affaires Scientifiques Techniques et Culturelles, PRODEX ESA, the Fond National de la Recherche Scientifique, and the Patrimoine de l'Université de Liège.

REFERENCES

1. Jaenicke R, Böhm G. The stability of proteins in extreme environments. Curr Opin Struct Biol 1998;8:738–748.
2. Russell RJM, Gerike U, Danson MJ, Hough DW, Taylor GL. Structural adaptations of the cold-active citrate synthase from an Antarctic bacterium. Structure 1998;6:351–361.
3. Alvarez M, Zeelen JP, Mainfroid V, et al. Triose-phophate isomerase (TIM) of the psychrophilic bacterium *Vibrio marinus*. J Biol Chem 1998;273:2199–2206.
4. Aghajari N, Feller G, Gerday C, Haser R. Structure of the psychrophilic *Alteromonas haloplanctis*α-amylase give insight into cold adaptation at a molecular level. Structure 1998;6:1503–1516.
5. Querol E, Perez-Pons JA, Mozo-Villarias A. Analysis of protein conformational characteristics related to thermostability. Protein Eng. 1996;9:265–271.
6. Jaenicke R, Schurig H, Beaucamp N, Ostendorp R. Structure and stability of hyperstable proteins:glycolytic enzymes from hyperthermophilic bacterium *Thermotoga maritima*. Adv Protein Chem 1996;48:181–269.
7. Voght G, Argos P. Protein thermal stability: hydrogen bonds or internal packing. Folding Design 1997;2:S40–S46.
8. Knowles JR. To build an enzyme. Philos Trans R Soc Lond B Biol Sci 1991;B332:115–121.
9. Noble MEM, Zeelen JP, Wierenga RK. Structure of the open and closed state of trypanosomal triosephosphate isomerase, as observed in a new crystal form: implications for the reaction mechanism. Proteins 1993;16:311–326.
10. Joseph D, Petsko GA, Karplus M. Anatomy of a conformational change: Hinged "lid" motion of the triose phosphate isomerase loop. Science 1990;249:1425–1428.
11. Schliebs W, Thanki, N, Eritja R, Wierenga R. Active site properties of monomeric triosephosphate isomerase (monoTIM) as deduced from mutational and structural studies. Protein Sci 1996;5:229–239.
12. Banner DW, Bloomer AC, Petsko GA, et al. Structure of chicken muscle triose phosphate isomerase determined crystallographically at 2.5 Å resolution. Nature 1975;255:609–614.
13. Wierenga RK, Noble MEM, Davenport RC. Comparison of the refined crystal structures of liganded and the unliganded chicken, yeast and trypanosomal triosephosphate isomerase. J Mol Biol 1992;224:1115–1126.
14. Lolis E, Alber T, Davenport RC, Rose D, Hartman FC, Petsko GA. Structure of yeast triosephosphate isomerase at 1.9 Å resolution. Biochemistry 1990;29:6609–6618.
15. Wierenga RK, Noble MEM, Vriend G, Nauche S, Hol WGJ. Refined 1.83Å structure of trypanosomal triosephosphate isomerase crystallized in the presence of 2.4M-ammonium sulphate. J Mol Biol 1991;220:995–1015.
16. Noble MEM, Zeelen JP, Wierenga RK. Structure of triosephosphate isomerase from *Escherichia coli* determined at 2.6Å resolution. Acta Crystallogr 1993;D49:403–417.
17. Mande SC, Mainfroid V, Kalk KH, Goraj K, Martial JA, Hol WGJ. Crystal structure of recombinant human triosphosphate isomerase at 2.8 Å resolution. Triosephosphate isomerase-related human genetic disorders and comparison with the trypanosomal enzyme. Protein Sci 1994;3:810–821.
18. Velanker SS, Ray SS, Gokhale RS, Hemalatha Balaram SS, Murthy MRN. Triosephosphate isomerase from *Plasmodium falciparum*: the crystal structure provides insights into antimalarial drug design. Structure 1997;5:751–761.
19. Williams JC, Zeelen JP, Neubauer G, Vriend G, Backmann J, Michels PA, Lambeir AM, Wierenga RK. Structural and mutational studies of leishmania triosephosphate isomerase: a point mutation can convert a mesophilic enzyme into a superstable enzyme without losing catalytic power. Prot Eng 1999;12:243.
20. Maldonado E, Soriano-Garcia M, Moreno A, et al. Differences in the intersubunit contacts in triosephosphate isomerase from two closely related pathogenic trypanosomes. J Mol Biol 1998;283:193–203.
21. Delboni LF, Mande SC, Rentier-Delrue F, et al. Crystal structure of recombinant triosephosphate isomerase from *Bacillus stearothermophilus*. An analysis of potential thermostability factors in six isomerases with known three-dimensional structures points to the importance of hydrophobic interactions. Protein Sci 1995;4:2594–2604.
22. Schurig H, Beaucamp N, Ostendorp R, Jaenicke R, Adler E, Knowles JR. PGK and TIM from the hyperthermophilic bacterium *Thermotoga maritima* form a covalent bifunctional enzyme complex. EMBO J 1995;14:442–452.
23. Beaucamp N, Hofmann A, Kellerer B, Jaenicke R. Dissection of the gene of the bifunctional PGK-TIM fusion protein from the hyperthermophilic bacterium *Thermotoga maritima*: design and characterization of the separate triosephosphate isomerase. Protein Sci 1997;6:2159–2165.
24. Yphantis DA. Equilibrium ultracentrifugation of dilute solutions. Biochemistry 1994;3:297–317.
25. Otwinowski Z. DENZO. An oscillation data processing program

for macromolecular crystallography. New Haven: Yale University Press; 1993.
26. Collaborative Computational Project Number 4. The CCP4 suite: programs for protein crystallography. Acta Crystallogr D 1994;D50: 760–763.
27. Navazza J. AMoRe: an automated package for molecular replacement. Acta Crystallogr 1994;A50:157–163.
28. Jones TA, Zou JY, Cowan SW, Kjelgaard M. Improved methods for building protein models in electron density amps and the location of errors in these models. Acta Crystallogr 1991;A47:110–119.
29. Brünger AT. X-PLOR. Version 3.1. A system for X-ray crystallography and NMR. New Haven: Yale University Press; 1992.
30. Brünger AT, Adams PD, Clore MG, et al. Crystallography & NMR system: a new software suite for macromolecular structure determination. Acta Crystallogr D 1998;D54:905–921.
31. Laskowski RA, MacArthur MW, Moss DS, Thornton JM. PROCHECK: a program to check the stereochemical quality of protein structures. J Appl Crystallogr 1993;26:283–291.
32. Vriend G. WHAT IF: a molecular modeling and drug design program. J Mol Graph 1990;8:52–56.
33. Devereux J, Haeberli P, Smithies O. A comprehensive set of sequence analysis programs for the VAX. Nucleic Acids Res 1984;12:387–395.
34. Kabsch W, Sander C. Dictionary of protein secondary structure: pattern recognition of hydrogen-bonded and geometrical features. Biopolymers 1983;22:2577–2637.
35. Richardson JS, Richardson DC. Amino acid preferences for specific locations at the ends of α helices. Science 1988;240:1648–1652.
36. Connolly ML. Computation of molecular volume. J Am Chem Soc 1985;107:1118–1124.
37. Hubbard SJ, Thornton JM. NACCESS [computer program]. Department of Biochemistry and Molecular Biology, University College, London; 1993.
38. McDonald I, Thornton J. Satisfying hydrogen bonding potential in proteins. J Mol Biol 1994;238:777–793.
39. Barlow DJ, Thornton MJ. Ion-pairs in proteins. J Mol Biol 1983;168:867–885.
40. Edsall JT. The size, shape and hydration of protein molecules. In: The proteins. Chemistry, biological activity and methods. New York: Neurath & Bailey;1953. p 636.
41. Durchschlag H, Jaenicke R. Partial specific volume changes of proteins: densimetric studies. Biochem Biophys Res Commun 1982;108:1074–1079.
42. Kohlhoff M, Dahm A, Hensel R. Tetrameric triosephosphate isomerase from hyperthermophilic Archaea. FEBS Lett 1996;383: 245–250.
43. Bell GS, Russell RJM, Kohlhoff M, et al. Preliminary crystallographic studies of triosephosphate isomerase (TIM) from the hyperthermophilic Archaeon *Pyrococcus woesei*. Acta Crystallogr 1998;D54:1419–1421.
44. Das G, Hickey DR, McLendon D, McLendon G, Sherman F. Dramatic thermostabilisation of yeast iso-1-cytochrome c by an asparagine => isoleucine replacement at position 57. Proc Nat. Acad Sci USA 1989;86:496–499.
45. Van den Burg B, Vriend G, Veltman OR, Venema G, Eijsink VGH. Engineering an enzyme to resist boiling. Biochemistry 1998;95: 2056–2060.
46. Usher KC, de la Cruz AFA, Dahlquist FW, Swanson RV, Simon MI, Remington SJ. Crystal structures of CheY from *Thermotoga maritima* do not support conventional explanations for the structural basis of enhanced thermostability. Protein Sci 1998;7:403–412.
47. Böhm G, Jaenicke R. Relevance of sequence statistics for the properties of extremophilic proteins. Int J Pept Protein Res 1994;43:97–106.
48. Matthews BW, Nicholson H, Becktel WJ. Enhanced thermostability from site-directed mutations that decrease the entropy of unfolding. Proc Natl Acad Sci USA 1987;84:6663–6667.
49. Russell RJM, Taylor GL. Engineering thermostability: lessons from thermophilic proteins. Curr Opin Biotech 1995;9:370–374.
50. Petukhov L, Kil Y, Kuramitsu S, Lanzov V. Insights into thermal resistance of proteins from intrinsic stability of their α-helices. Proteins 1997;29:309–320.
51. Facchiano AM, Colonna G, Ragone R. Helix stabilizing factors and stabilization of thermophilic proteins: an X-ray based study. Protein Eng 1998;11:753–760.
52. Nicholson H, Becktel W, Matthews BW. Enhanced protein thermostability from designed mutations that interact with α-helix dipoles. Nature 1988;336:651–656.
53. Serrano L, Fersht AR. Capping and α-helix stability. Nature 1989;342:296–299.
54. Lee B, Vasmatzis G. Stabilization of protein structures. Curr Opin Struct Biol 1997;8:423–428.
55. Dill KA. Dominant forces in protein folding. Biochemistry 1990;29: 7133–7155.
56. Eisenberg D, McLachlan AD. Solvation energy in protein folding and binding. Nature 1986;319:199–203.
57. Xie D, Freire E. Molecular basis of cooperativity in protein folding. Thermodynamic and structural conditions for the stabilization of compact denatured states. Proteins 1994;19:291–301.
58. Dahiyat BI, Mayo SL. Protein design automation. Protein Sci 1996;5:895–903.
59. Backmann J, Schäfer G, Wyns L, Bönisch H. Thermodynamics and kinetics of unfolding of the trimeric adenylate kinase from the archeon *Sulfolobus acidocaldarius*. J Mol Biol 1998;284:817–833.
60. Tanner JT, Hecht RM, Krause KL. Determinants of enzyme thermostability observed in the molecular structure of *Thermus aquatus* D-glyceraldehyde-3-phosphate dehydrogenase at 2.5Å resolution. Biochemistry 1996;35:2597–2609.
61. Perutz MF, Raidt H. Stereochemical basis of heat stability in bacterial ferredoxins and in haemoglobin A2. Nature 1975;255: 256–259.
62. Goldman A. How to make my blood boil. Structure 1995;3:1277–1279.
63. Yip KSP, Stillman TJ, Britton KL, et al. The structure of *Pyrococcus furiosus* glutamate dehydrogenase reveals a key role for ion-pair networks in maintaining enzyme stability at extreme temperatures. Structure 1995;3:1147–1158.
64. Vetriani C, Maeder DL, Tolliday N, et al. Protein thermostability above 100°C: a key role for ionic interactions. Proc Natl Acad Sci USA 1998;95:12300–12305.
65. Nakashima H, Nishikwa K, Ooi T. The folding type of a protein is relevant to the amino acid composition. J Biochem 1986;99:153–162.